Geophysical Research Letters

RESEARCH LETTER
10.1029/2020GL088761

Key Points:
- We illustrate the differences between and similarities of the electron-only reconnection and the normal reconnection
- The electron reconnection was prior to the normal reconnection
- The Hall electric field and the reconnected magnetic field intensity could control the form of reconnection

Correspondence to:
R. Wang and Q. Lu,
rswan@ustc.edu.cn;
qmlu@ustc.edu.cn

Citation:
Wang, R., Lu, Q., Lu, S., Russell, C. T., Burch, J. L., Gershman, D. J., et al. (2020). Physical implication of two types of reconnection electron diffusion regions with and without ion-coupling in the magnetotail current sheet. *Geophysical Research Letters*, *47*, e2020GL088761. https://doi.org/10.1029/2020GL088761

Received 6 MAY 2020
Accepted 21 OCT 2020
Accepted article online 29 OCT 2020

Physical Implication of Two Types of Reconnection Electron Diffusion Regions With and Without Ion-Coupling in the Magnetotail Current Sheet

Rongsheng Wang[1,2,3], Quanming Lu[1,2,3], San Lu[4], Christopher T. Russell[4], J. L. Burch[5], Daniel J. Gershman[6], W. Gonzalez[7], and Shui Wang[1,2,3]

[1]CAS Key Laboratory of Geospace Environment, Department of Geophysics and Planetary Science, University of Science and Technology of China, Hefei, China, [2]CAS Center for Excellence in Comparative Planetology, Hefei, China, [3]Anhui Mengcheng Geophysics National Observation and Research Station, University of Science and Technology of China, Mengcheng, China, [4]Earth Planetary and Space Sciences, University of California, Los Angeles, CA, USA, [5]Southwest Research Institute, San Antonio, TX, USA, [6]NASA, Goddard Space Flight Center, Greenbelt, MD, USA, [7]Instituto Nacional de Pesquisas Espaciais, São Paulo, Brazil

Abstract By comparing an electron-only reconnection event with a traditional reconnection event observed in the magnetotail, we illustrate the differences between and similarities of the two events. The electron behaviors are very similar in both events, but intensities of the electron flows and temperature in the traditional reconnection are much stronger than those in the electron-only reconnection. The Hall electric field in the traditional reconnection occurs on the ion-scale and is deflected from the normal direction by the significant magnetic field reconnected, while this field varies on the electron-scale and points to the middle plane in the electron-only reconnection. The comparison indicates that the electrons are undergoing the same process in both events, and the electron-only reconnection was prior to the traditional reconnection. The Hall electric field could control the form of reconnection: producing either electron-only reconnection or traditional reconnection.

1. Introduction

Magnetic reconnection is an important mechanism for converting magnetic energy into plasma energy. It generally occurs within a narrow boundary layer but affects large volumes from the terrestrial magnetosphere to the solar heliosphere (Yamada et al., 2010). The coupling between the reconnection and the large volumes in which it occurs has been extensively studied. In the vicinity of the reconnection site, ions and electrons become decoupled from the magnetic field in regions termed the ion and electron diffusion region (EDR), respectively, due to the Hall effect in the collisionless environment. The size of ion diffusion region (IDR) is much larger than EDR (Birn & Hesse, 2001; Ma & Bhattacharjee, 1998; Sonnerup, 1979). Thus, it is widely accepted that both the ions and electrons are involved simultaneously in the reconnection process. Recently, a new form of reconnection (Phan et al., 2018; Stawarz et al., 2019), where only the electrons participate in the process and the ions do not respond to it, was observed in the turbulent magnetosheath plasma. The relation between the electron-only reconnection and the traditional reconnection has been elusive.

The absence of ion response in the electron-only reconnection was attributed to the small scale of the current sheets in the magnetosheath, and thereby, there was not sufficient space and time for the ions to couple with the process (Phan et al., 2018). The transition from traditional reconnection to the electron-only reconnection was realized in the particle-in-cell simulations (Pyakurel et al., 2019). It is found that the ions did not respond to the reconnection dynamics when the reconnecting regions with scales was comparable to the ion inertial length. It seems that the transition was controlled only by the simulation domain size, namely, the scale of current sheet where the reconnection occurred. However, electron-only reconnection is observed as well in the near-Earth magnetotail (Wang et al., 2018), where the electron-scale current layer was embedded in a much broader ion-scale current sheet (Artemyev et al., 2013; Nakamura et al., 2006, 2008; Sergeev et al., 1993). This challenges the conclusion that the size of the current sheet determines whether the reconnection is either electron-only reconnection or traditional reconnection.

In this letter, by examining one reconnection event without ion-coupling (Wang et al., 2018) and the other with ion-coupling (Li et al., 2019; Zhou et al., 2019) in the magnetotail, we determine the differences between and similarities of the two events. Based on the comparison, we propose that the two forms of reconnection correspond to two different stages of reconnection in the macroscale current sheet of the magnetotail and examine the potential factors controlling the transition between the two stages.

2. Instrumentation

The Magnetospheric Multiscale mission (MMS) (Burch et al., 2016) consists of the four satellites equipped with the identical instruments, including the magnetometer (Russell et al., 2016), the fast plasma instruments (FPI) (Pollock et al., 2016), and electric field instruments (Ergun et al., 2016; Lindqvist et al., 2016). The magnetic field is sampled at 128/s (Russell et al., 2016), and the electric field is sampled at 8,192/s (Ergun et al., 2016; Lindqvist et al., 2016) in burst mode. The time resolutions for electrons and ions taken from the FPI in burst mode are 30 and 150 ms, respectively. In this letter, we utilized the higher time resolution plasma data (7.5 ms for electrons and 37.5 ms for ions), obtained by reducing the azimuthal sampling resolution and the details can be found in Rager et al. (2018).

3. Observation and Analysis

Figure 1 shows the two reconnection events observed during 20:24:03–20:24:11 UT on 17 Jun 2017 (dubbed Event I, left column), when the spacecraft was located at [−19.4, −10.4, 5.5] R_e in the Geocentric Solar Ecliptic (GSE) coordinate system with a separation of ~30 km, and during 12:18:00–12:19:00 UT on 10 August 2017 (Event II, right column), at [−15.3, 2.7, 4.8] R_e with a separation of ~20 km. Since the spacecraft separation was small, we used the data from MMS2, except for the velocity at the barycenter of the four satellites in Figure 4 where the data at all four satellites have to be used. In both events, the spacecraft crossed the magnetotail plasma sheet from the south hemisphere to the north hemisphere and detected an extremely strong current enhancement, up to 200 nA/m^2, at its center (Figures 1e and 1m). These strong currents were verified to be carried by the electrons (Li et al., 2019; Huang et al., 2018; Wang et al., 2018; Zhou et al., 2019) and will be analyzed later in their individual local current coordinates.

The local current system in Event I was derived from minimum variance analysis (Paschmann & Schwartz, 2000), with $\mathbf{L}$ = [0.9477, 0.3023, −0.1029], $\mathbf{M}$ = [−0.0855, −0.0703, −0.9939], and $\mathbf{N}$ = [−0.3076, 0.9506, −0.0408] relative to the GSE. In Event II, a hybrid method of minimum variance analysis and maximum direction derivative (MDD) (Shi et al., 2005) was used to obtain the local current system, $\mathbf{L}$ = [0.9617, −0.1762, −0.2099], $\mathbf{M}$ = [0.2522, 0.8686, 0.4266], and $\mathbf{N}$ = [0.1071, −0.4632, 0.8798]. The details on the choice of the local current system can be found in Li et al. (2019). Because the four MMS satellites passed through the electron current layers one after another, the Timing method (Schwartz, 1998) was used to estimate the current layer velocity and the thickness. In Event I, the speed was ~67.0 km/s, the duration was ~2.0 s, (20:24:06.3–20:24:08.3 UT, Figures 1b and 1e), and its half-width was ~67 km ~9.0 d_e, where the electron inertial length d_e = 7.5 km based on N_e = 0.5 cm^{-3}. In Event II, the speed was ~38.4 km/s, the duration in the south part of the current layer was ~3.0 s (12:18:30–12:18:33 UT, Figures 1j and 1m), and the half-width was ~9.7 d_e, where d_e = 11.9 km based on N_e = 0.2 cm^{-3}.

In Event I, the electron-scale current layer was observed without any bursty reconnection signature, i.e., without the expected ion bursty bulk flows (Wang et al., 2018). In order to confirm whether the absence of the ion flows was due to the insufficient time resolution of the data, the higher time resolution plasma data (7.5 ms for electrons and 37.5 ms for ions) was used, four times faster than the data in burst mode (Pollock et al., 2016). Based on these new data, we confirmed that the electron-scale current layer was actually an EDR. During the layer crossing in Event I (Figure 1b), the super-Alfvénic electron jet (v_{eL} > 1,000 km/s ~ 2.0 v_A, v_{eM} > 2,300 km/s ~ 5.0 v_A ~ 0.12 v_{eA}, where $v_A \approx 460$ km/s and $v_{eA} \approx 2.0 \times 10^4$ km/s are Alfvénic and electron Alfvénic speeds based on N_e = 0.5 cm^{-3} and B = 15 nT, Figure 1d), the intense current density (Figure 1e), the Hall electric field (red trace in Figure 1f), and Hall magnetic field (blue trace in Figure 1b) were observed. These 7.5 ms cadence data show that $|v_{e\perp}|$ was strong in the layer (up to 2,000 km/s, Figure 2a) and displayed a double-peaked structure with a dip at the layer center (20:24:07 UT). $v_{e//}$ was weak and had a minor peak (~1,000 km/s) at the center. $\mathbf{V}_{e\perp}$ shows a clear deviation from $\frac{\mathbf{E}\times\mathbf{B}}{\mathbf{B}^2}$ (Figures 2b–2d),

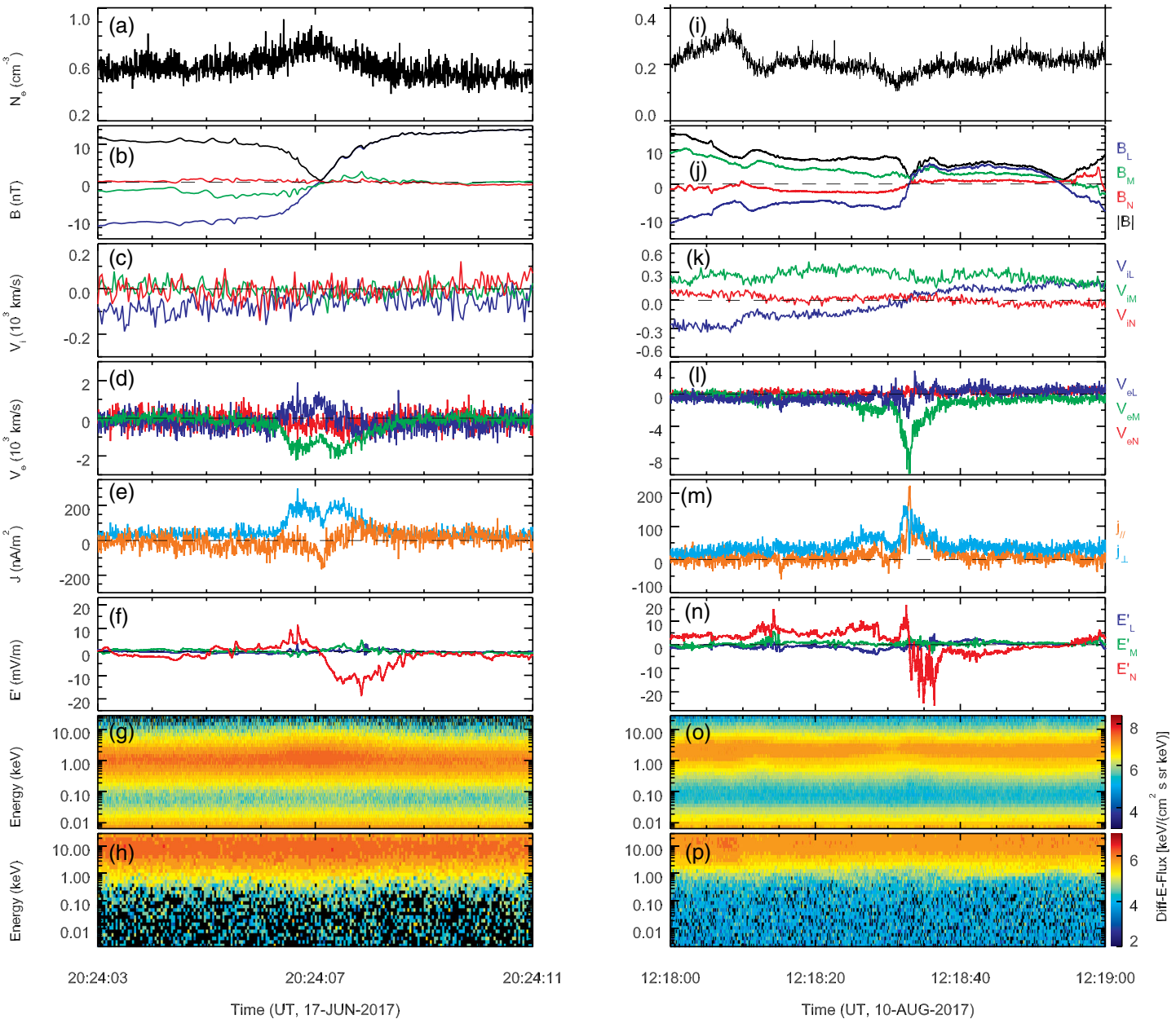

Figure 1. (a–h) From top to bottom, electron density, three components and intensity of magnetic field, ion bulk flow vector, electron bulk flow, electron current density, three components of electric field in the frame of the current sheet, electron, and ion energy spectrum in Event I. (i–p) The data in Event II, in the same format as (a)–(h).

especially in the *M* direction. This means that the electrons were decoupled from magnetic field therein. In Event I, both $T_{e//}$ and $T_{e\perp}$ were enhanced (Figure 2e), and the energy dissipation $\mathbf{J}\cdot(\mathbf{E}+\mathbf{V}_e\times\mathbf{B})$ (Figure 2f) was significant: positive (~0.2 nW/m^2) around the layer center and negative out of the center, consistent with the simulation results where positive $\mathbf{J}\cdot(\mathbf{E}+\mathbf{V}_e\times\mathbf{B})$ was surrounded by negative values around the X-line (Zenitani et al., 2011) as well as the low-shear EDR (Genestreti et al., 2017), and the crescent distribution in the $v_{e\perp1}-v_{e\perp2}$ plane (Figure 4a) (where $\mathbf{V}_{e\perp1}=\frac{(\mathbf{B}\times\mathbf{V}_e)\times\mathbf{B}}{\mathbf{B}^2}$ and $\mathbf{V}_{e\perp2}=\frac{\mathbf{B}\times\mathbf{V}_e}{\mathbf{B}}$), as an indication of in the EDR proximity (Burch et al., 2016; Egedal et al., 2016; Hesse et al., 2014; Li et al., 2019; Torbert et al., 2018), was observed. Thus, we conclude that the current layer in Event I was an EDR. The super-

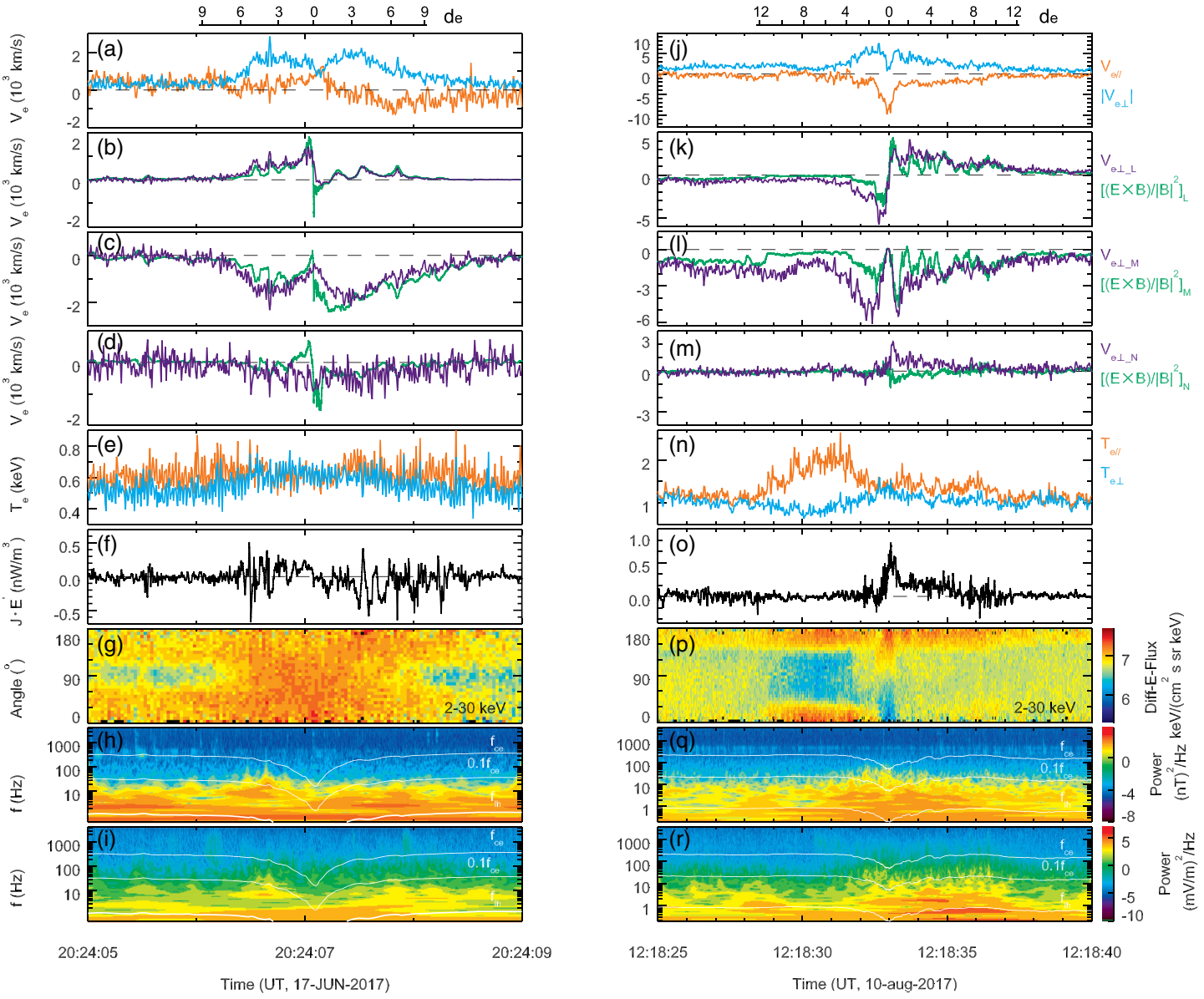

Figure 2. The left and right columns correspond to Events I and II, respectively. (a) $v_{e//}$, $|v_{e\perp}| = |\frac{\mathbf{B}\times(\mathbf{v}_e\times\mathbf{B})}{\mathbf{B}^2}|$, (b–d) three components of $\frac{\mathbf{B}\times(\mathbf{v}_e\times\mathbf{B})}{\mathbf{B}^2}$ and $\frac{\mathbf{E}\times\mathbf{B}}{\mathbf{B}^2}$. (e) $T_{e//}$ and $T_{e\perp}$, (f) $\mathbf{J}\cdot(\mathbf{E}+\mathbf{V}_e\times\mathbf{B})$, (g) electron pitch angle distribution at energies 2–30 keV. (h–i) Magnetic field and electric field power spectral densities according to the wavelet technique. (j–r) The data in the same format.

Alfvénic electron jet and the negative-then-positive variation of B_M suggest that MMS traversed the EDR earthward of the X-line (Wang et al., 2018), as illustrated in Figure 3a. However, the expected earthward ion outflows were not observed, even at the 37.5-ms cadence. On the contrary, a weak tailward ion flow, $v_{iL} \sim -100$ km/s, was detected (Figure 1c). It appears that this EDR was not coupled with the ions, analogous to the electron-only reconnection in the magnetosheath (Phan et al., 2018; Stawarz et al., 2019) and in the associated boundary (Norgren et al., 2018).

In order to reveal the differences and similarities between EDRs with and without ion-coupling in the magnetotail, a traditional reconnection event (Event II) is presented (Figures 1i–1p). The super-Alfvénic electron jets are detected at the center (Figure 1l, v_{eL} changed sign from negative to positive, $|v_{eL}|$ up to 2,000 km/s, ~2.4 v_A; v_{eM} was directed in the $-M$ direction, ~−10,000 km/s ~−12.1v_A, ~−0.28 v_{eA}, where $v_A = 829$ and

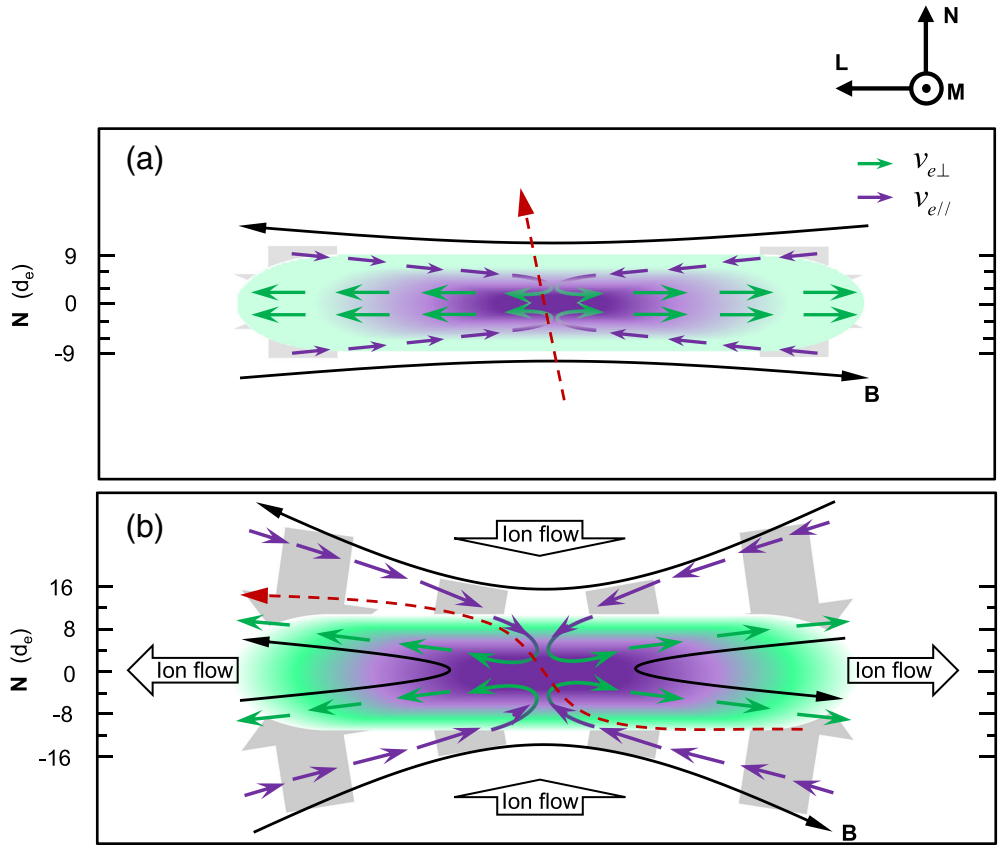

Figure 3. (a and b) Schematic illustrations for Events I and II, respectively. The red lines show the MMS trajectories. The Hall electric field is denoted by the wide gray arrows.

$v_{eA} = 3.6 \times 10^4$ km/s based on $N_e = 0.2$ cm^{-3} and $B = 17$ nT), as the spacecraft traverses the layer (Figure 1j). The perpendicular current density $|j_\perp|$ displays a bifurcated structure (more evident in Figure 2j) and $j_{//}$ peaked at the layer center (Figure 1m), which is similar to Event I. The evident signatures of Hall electric (Figure 1n) and magnetic field (Figure 1j), the significant deviation between $\mathbf{v}_{e\perp}$ and $\frac{\mathbf{E}\times\mathbf{B}}{\mathbf{B}^2}$ (Figures 2k–2m), the rapid growth of the electron temperature $T_{e\perp}$ and $T_{e//}$ (Figure 2n), the intense energy dissipation (>0.7 nW/m^2, Figure 2o), and the clear electron crescent distribution (Figure 4e) indicate an encounter of the EDR. These observational features are exactly analogous to those in Event I, except for their intensities. This indicates that the electron dynamics in both events were subjected to the same physical process.

One striking distinction between the two events is the ion behavior. In Event II, as the spacecraft passed through the EDR, the ion flow v_{iL} reversed from negative to positive, and v_{iM} was continuously positive (Figure 1k), opposite to v_{eM}. This means that MMS crossed the EDR from tailward to earthward. The weak v_{iL} ($|v_{iL}| < 300$ km/s ~ 0.4 v_A) indicates that the spacecraft was very close to the X-line and the ions had not been effectively accelerated. v_{iN} was basically positive in the south and became negative in the north (Figure 1k), suggesting that the ions were moving towards the middle plane on both sides of the EDR. In other words, the ion inflows were observed. The spacecraft trajectory in Event II was present in Figure 3b. In contrast, $v_{iN} \approx 0$, $v_{iM} \approx 0$ (Figure 1c), and v_{iL} were weakly tailward in Event I. Namely, inflowing ions were not observed ($v_{iN} \sim 0$), even though the spacecraft crossed the EDR.

There were other differences between the two events as well. The density in Event I (~0.5 cm^{-3}) was denser than that in Event II (~0.2 cm^{-3}). A density peak (~0.8 cm^{-3}) was obvious in the layer center of Event I (Figure 1a) while a density minimum (~0.14 cm^{-3}) was observed at the center of Event II (Figure 1i). The

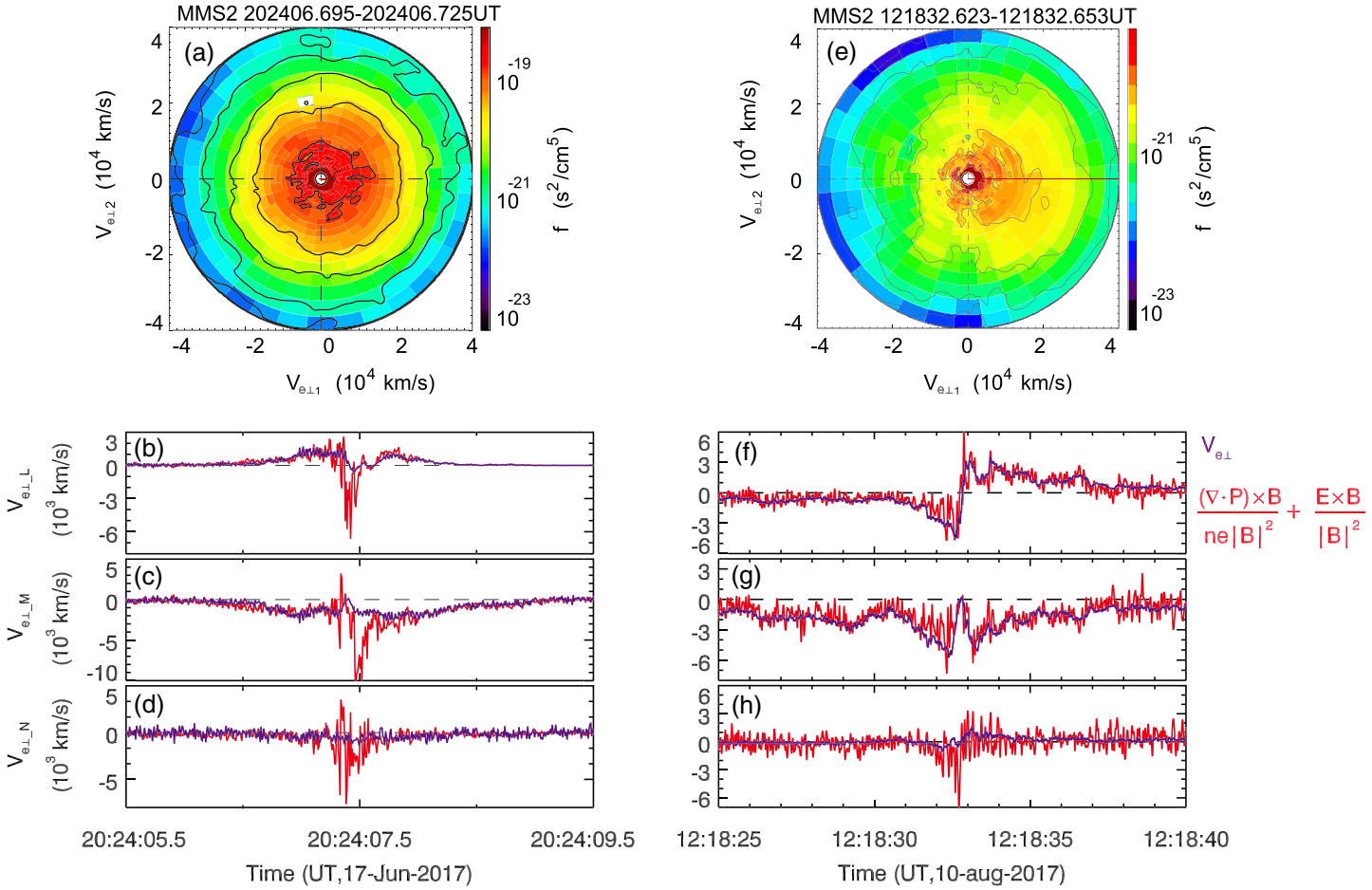

Figure 4. Panels (a)–(d) show the data in Event I. (a) Electron distribution in the perpendicular plane ($\mathbf{V}_{e\perp1} = \frac{(\mathbf{B}\times\mathbf{V}_e)\times\mathbf{B}}{\mathbf{B}^2}$, $\mathbf{V}_{e\perp2} = \frac{\mathbf{B}\times\mathbf{V}_e}{\mathbf{B}}$). (b–d) Electron perpendicular velocity and $\frac{\nabla\cdot\mathbf{P}\times\mathbf{B}}{en\mathbf{B}^2} + \frac{\mathbf{E}\times\mathbf{B}}{\mathbf{B}^2}$ at the barycenter of the four satellites. Panels (e)–(h) show the data in Event II.

magnetic field magnitude in the plasma sheet boundary was more or less the same in both events. The asymptotic value was ~15 nT in Event I and ~17 nT in Event II (not shown). The profiles of the electron velocity (Figures 1d and 1l and 2a and 2j) and current density (Figures 1e and 1m) across the EDR were extremely similar in both events. However, the peak value of v_{eM} (~5.0 v_A) in Event I was much weaker than that (~12.1 v_A) in Event II. The current density did not exhibit the dramatic difference as the density and velocity between the two events. The maximum value of $|j_\perp|$ in Event I (~250 nA/m^2) was stronger than that (~150 nA/m^2) in Event II. On the contrary, the peak value of $|j_{//}|$ (~150 nA/m^2) in Event I was weaker than that (~220 nA/m^2) in Event II.

The electron pitch angle distribution also displayed a slight difference in the two events. The electron differential fluxes were depleted at just ~90°, out of the EDR (before 20:24:06.4 and after 20:24:08 UT) in Event I (Figure 2g), leading to a bidirectional field-aligned distribution, but the flux enhancements were observed in a wide range (~0°–60° and ~120°–180°) rather than just along the magnetic field (~0° and 180°). Inside the EDR of Event I, the fluxes at the angles less than 90° were slightly higher than those in other directions (>90°) inside the EDR, resulting in the $v_{e//}$ peak at the layer center (Figure 2a). During Event II, the flux depletion was detected in a much wider range, from 30° to 150° (12:18:28.0–12:18:32.5 UT), and flux enhancement was observed mainly along the magnetic field (0°–30° and 150°–180°), i.e., the bidirectional field-aligned distribution, in the tailward part (Figure 2p), while the distribution was replaced by the enhancement antiparallel to the magnetic field in the north part (12:18:33.5–12:18:38.0 UT) due to the appearance of the large-amplitude fluctuations of the electric field (Li et al., 2019). At the EDR center of

Event II (~12:18:34 UT), the beam-like electron distribution was observed mainly antiparallel to the magnetic field and produced a strong electron flow $v_{e//}$ (Figure 2j). It is clear that the electrons were pulled more towards the magnetic field line direction in the traditional reconnection than in the electron-only reconnection. $T_{e//}$ and $T_{e\perp}$ in both events (Figures 2e and 2n) displayed a very similar profile across the EDR, i.e., $T_{e\perp}$ peaked at the EDR center while $T_{e//}$ had a dip there, in good agreement with the simulation results (Shay et al., 2014).

The Hall electric field $E_N^{'}$ in the frame of the EDR was less than 20 mV/m and confined to the electron current layer in Event I (Figure 1f), and thus, the width of the Hall electric field was ~9 d_e. In Event II, the Hall field became stronger (up to 25 mV/m) and was constantly observed during the whole crossing (Figure 1n), other than just inside the electron current layer. $E_N^{'}$ retained ~−4 mV/m when MMS was located in the boundary of the current layer ($B_L \approx 17$ nT). Assuming pressure balance across the plasma sheet, we can roughly estimate its thickness by the Ampère's law. The half-width of the plasma sheet maintained above 1,000 km before 12:18:25 and after 12:18:40 UT, when the Hall electric field was still evident. Thus, the width of the Hall electric field was at least 500 km ~ 1.0 d_i, significantly wider than that in Event I. Although the width of the Hall electric field was different in both events, the thicknesses of the electron current layers were nearly equal to ~9 d_e, consistent with the laboratorial results (Ji et al., 2008). More importantly, $E_L^{'}$, as one component of the Hall electric field due to the significant value of B_N (Figure 1j), was negative in the tailward of the X-line and became positive earthward of the X-line in the Event II (Figure 1n). In contrast, $E_L^{'}$ was negligible in Event I.

Based on the generalized Ohm's law (Vasyliunas, 1975), the perpendicular electron velocity components can be from the convection term, the electron pressure tensor term, and the electron inertial term since the classical resistivity term was generally negligible. The difference between $\mathbf{v}_{e\perp}$ and $\frac{\mathbf{E}\times\mathbf{B}}{\mathbf{B}^2}$ was large in both events, and it was more significant in Event II (Figures 2k–2m) than that in Event I (Figures 2b–2d). Given the diamagnetic drift ($\frac{(\nabla\cdot\mathbf{P}^{\rightarrow})\times\mathbf{B}}{ne\mathbf{B}^2}$), $\mathbf{v}_{e\perp}$ and $\frac{(\nabla\cdot\mathbf{P}^{\rightarrow})\times\mathbf{B}}{ne\mathbf{B}^2}+\frac{\mathbf{E}\times\mathbf{B}}{\mathbf{B}^2}$ matched well in Event II (Figures 4f–4h), and also in Event I, even in the 7.5 ms cadence (Figures 4b–4d) except for at the very center of EDR (~300 ms, from 20:24:07.3 to 20:24:07.6 UT). The disagreement during this ~300 ms of interval was much larger than the deviation between $\mathbf{v}_{e\perp}$ and $\frac{\mathbf{E}\times\mathbf{B}}{\mathbf{B}^2}$ (Figures 2b–2e) and could be artificial due to the narrow spatial scale (~20 km) being less than the spacecraft separation (~30 km) (Wang et al., 2018). As a result, the perpendicular electron flows in both EDRs were primarily generated by the combination of electric field drift and diamagnetic drift.

4. Discussion and Conclusion

The electron-only reconnection was first observed in the magnetosheath turbulent plasma where the electron-scale reconnecting current sheet was not embedded inside a much larger ion-scale current layer (Phan et al., 2018). Due to the absence of a wider ion-scale current layer, it is reasonable that no ions responded to the electron-scale reconnecting current layer. However, the electron-scale current layer in the magnetotail must be embedded inside a much broader ion-scale current sheet. The gradual increase of magnetic field intensity as MMS left the centers indicates that there was a broad ion current sheet in both events (Wang et al., 2018). Thus, there is no reason that the ions detached themselves from the reconnection process. By comparing the two EDR events with and without ion-coupling, we find that the profiles of the electron flows ($v_{e//}$, $|v_{e\perp}|$), the current density ($j_{//}$, $|j_{\perp}|$), and electron temperature ($T_{e//}$,$T_{e\perp}$) across the EDR were very similar, except for their intensities. $v_{e\perp}$, $v_{e//}$ and $j_{//}$ were much stronger in the traditional reconnection than those in the electron-only reconnection.

In both EDR events, the perpendicular electron flows were caused by the electric field drift and the diamagnetic drift. The contribution from the diamagnetic drift became more and more important in the traditional reconnection than in the electron-only reconnection. The parallel electron flows were observed in both EDR events and reached maximum value at the center of the EDR. The parallel electron speed in the traditional reconnection (~12.1 v_A) was much stronger than that (~2.0 v_A) in the electron-only reconnection. It is believed that the electrons are effectively accelerated by the parallel potential during reconnection (Egedal

et al., 2009, 2012) and thereby the electron parallel speed gradually increases as the reconnection proceeds. Therefore, it seems that the electrons in the traditional reconnection event and electron-only reconnection event were subjected to the same process, i.e., reconnection, but in distinct stages, and the electron-only reconnection was in the early stages of reconnection. If so, the electron temperature would be higher in the traditional reconnection than in the electron-only reconnection, consistent with the fact. In addition, the energy dissipation was more efficient in the traditional reconnection as well. However, the plasma parameters, e.g., the density and temperature, varied largely at different times in the magnetotail, which can cause the differences between the two events analyzed as well. At present, we cannot exclude such possibility.

One may be concerned that the observed differences between two events could be caused by the different trajectories relative to the X-line. Specially, one would not expect to see the strong outflows and the significant reconnected magnetic field if the spacecraft crossed the EDR center along the normal direction as the case in Event I. In other words, MMS directly crossed the EDR very close to its center and thus was not able to detect the strong outflows and reconnected field even if they had been created downstream of the EDR in Event I. Given Event II of the classic reconnection where MMS crossed the EDR from lower-right quadrant to the upper-left quadrant and detected the inflowing and outflowing ions simultaneously, MMS in Event I should have detected the inflowing ions while it crossed the EDR center along the normal. The fact is that the expected ion inflowing were not observed in Event I. Therefore, we excluded this possibility.

Since the ions and electrons were decoupled from the magnetic field in the EDR, the ions could respond to the reconnection process only via electrostatic interaction. In electron-only reconnection, the Hall electric field was restricted within the electron-scale layer and primarily pointed to the normal direction due to the negligible magnetic field in this direction, and therefore, it could not create ion bulk flows in the normal direction, namely, the ion inflows and also in the outflow direction, i.e., the ion outflows, since the ion gyro radius was larger than the width of the Hall electric field. In contrast, the Hall electric field has broadened to be ion-scale in the traditional reconnection, even though the electron current layer retained an electron-scale. Hence, the ions can be accelerated to form the inflow (Wygant et al., 2005; Yoo et al., 2014). In addition, the reconnected magnetic field along the normal direction was significant in the traditional reconnection, and thereby, a component of the Hall electric field was created in the outflow directions (blue trace in Figure 1n), generating the ion outflows. It appears that the width of the Hall electric field was the main factor controlling the transition from electron-only reconnection to the traditional reconnection if the transition could really happen. Then, the transition should be gradual as the Hall electric field region broadens. Most recently, the transition from the electron-only reconnection to the traditional reconnection was successively simulated in particle-in-cell simulations with a simulation domain much larger than the ion inertial length, supporting our speculation (Lu et al., 2020). In the simulation, the electron-only reconnection can persist for ~10 Ω_i^{-1}, where $\Omega_i = e \mid B \mid /m_i$ is ion cyclotron frequency, sufficiently long to be detected by MMS with a highly sampled rate.

In Event I, the M component was primarily along the Z direction of the GSE coordinates. Namely, the current layer was vertical to the equatorial plane ($x-y$ plane in GSE) (Wang et al., 2018), i.e., the so-called tilted current sheet (Baumjohann et al., 2007; Petrukovich et al., 2008; Vasko et al., 2014). In Event II, the current layer was mainly horizontal in the equatorial plane. Theoretically, it was realized very early that the electron tearing instability is stable in the magnetotail due to the weak normal magnetic field B_z (Lembege & Pellat, 1982; Pritchett & Lu, 2018; Sitnov & Schindler, 2010). Even so, the spontaneous tearing instability has been used to explain the reconnection onset in the magnetotail. The tilted current sheet can account for the discrepancy, since the normal magnetic field B_z changed to be the component in the plane of the tiled current layer, allowing the instability to occur spontaneously. This speculation is consistent with our observation of the electron-only reconnection, but more evidence is needed.

In both EDR, the electromagnetic radiation from f_{lh} to $0.1f_{ce}$ (Figures 2h–2i and 2q–2r) was observed, where f_{lh} is the lower hybrid frequency and f_{ce} is electron cyclotron frequency, and there were no higher frequency waves observed. In the electron-only reconnection, the strongest waves were primarily observed in the strong gradient of magnetic field or the sharp edges of the electron current layer (~20:24:06.7 and ~20:24:07.8 UT) and were weak in the current layer center (~20:24:07.0 UT, Figures 2h–2i). In the classical reconnection, the waves were detected in the whole current layer, including the layer center (Figures 2q–2r). The roles of these waves on the reconnection evolution are unclear.

Our results also raise other questions, e.g., how long would the electron-only reconnection continue and must the transition happen in the magnetotail? The different environments in the magnetotail and the magnetosheath may influence the transition. It could be that a complex turbulent environment will prevent the reconnection from proceeding to a classical reconnection with ion-coupling, while in a more laminar large-scale current sheet which may be the common situation in the magnetotail, the transition will occur.

Data Availability Statement

The data used in this work are available online (https://lasp.colorado.edu/mms/sdc/public/about/browse-wrapper/).

Acknowledgments
This work is supported by the National Science Foundation of China (NSFC) grants (41922030, 41674143, and 41527804), Key Research Program of Frontier Sciences, CAS (QYZDJ-SSW-DQC010), the B-type Strategic Priority Program of the Chinese Academy of Sciences (XDB41000000), and the Fundamental Research Funds for the Central Universities.

References

Artemyev, A. V., Petrukovich, A. A., Frank, A. G., Nakamura, R., & Zelenyi, L. M. (2013). Intense current sheets in the magnetotail: Peculiarities of electron physics. *Journal of Geophysical Research: Space Physics*, *118*, 2789–2799. https://doi.org/10.1002/jgra.50297

Baumjohann, W., Roux, A., le Contel, O., Nakamura, R., Birn, J., Hoshino, M., et al. (2007). Dynamics of thin current sheets: Cluster observations. *Annals of Geophysics-Germany*, *25*(6), 1365–1389. https://doi.org/10.5194/angeo-25-1365-2007

Birn, J., & Hesse, M. (2001). Geospace environment modeling (GEM) magnetic reconnection challenge: Resistive tearing, anisotropic pressure and Hall effects. *Journal of Geophysical Research*, *106*(A3), 3737–3750.

Burch, J. L., Torbert, R. B., Phan, T. D., Chen, L. J., Moore, T. E., Ergun, R. E., et al. (2016). Electron-scale measurements of magnetic reconnection in space. *Science*, *352*(6290), aaf2939. https://doi.org/10.1126/science.aaf2939

Egedal, J., Daughton, W., Drake, J. F., Katz, N., & Le, A. (2009). Formation of a localized acceleration potential during magnetic reconnection with a guide field. *Physics of Plasmas*, *16*(5).

Egedal, J., Daughton, W., & Le, A. (2012). Large-scale electron acceleration by parallel electric fields during magnetic reconnection. *Nature Physics*, *8*(4), 321–324.

Egedal, J., Le, A., Daughton, W., Wetherton, B., Cassak, P. A., Chen, L. J., et al. (2016). Spacecraft observations and analytic theory of crescent-shaped electron distributions in asymmetric magnetic reconnection. *Physical Review Letters*, *117*(18), 185101. https://doi.org/10.1103/PhysRevLett.117.185101

Ergun, R. E., Tucker, S., Westfall, J., Goodrich, K. A., Malaspina, D. M., Summers, D., et al. (2016). The axial double probe and fields signal processing for the MMS mission. *Space Science Reviews*, *199*(1–4), 167–188. https://doi.org/10.1007/s11214-014-0115-x

Genestreti, K. J., Petrukovich, A. A., Frank, A. G., Nakamura, R., & Zelenyi, L. M. (2017). The effect of a guide field on local energy conversion during asymmetric magnetic reconnection: MMS observations. *Journal of Geophysical Research: Space Physics*, *122*, 11,342–11,353. https://doi.org/10.1002/jgra.50297

Hesse, M., Aunai, N., Sibeck, D., & Birn, J. (2014). On the electron diffusion region in planar, asymmetric, systems. *Geophysical Research Letters*, *41*, 8673–8680. https://doi.org/10.1002/2014GL061586

Huang, S. Y., Jiang, K., Yuan, Z. G., Sahraoui, F., He, L. H., Zhou, M., et al. (2018). Observations of the electron jet generated by secondary reconnection in the terrestrial magnetotail. *The Astrophysical Journal*, *862*(2), 144. https://doi.org/10.3847/1538-4357/aacd4c

Ji, H., Ren, Y., Yamada, M., Dorfman, S., Daughton, W., & Gerhardt, S. P. (2008). New insights into dissipation in the electron layer during magnetic reconnection. *Geophysical Research Letters*, *35*, L13106. https://doi.org/10.1029/2008GL034538

Lembege, B., & Pellat, R. (1982). Stability of a thick two-dimensional quasi-neutral sheet. *Physics of Fluids*, *25*(11), 1995–2004.

Li, X. M., Wang, R. S., Lu, Q. M., Hwang, Y. O. O., Zong, Q. G., Russell, C. T., & Wang, S. (2019). Observation of nongyrotropic electron distribution across the electron diffusion region in the magnetotail reconnection. *Geophysical Research Letters*, *46*, 14,263–14,273. https://doi.org/10.1029/2019GL085014

Lindqvist, P. A., Olsson, G., Torbert, R. B., King, B., Granoff, M., Rau, D., et al. (2016). The spin-plane double probe electric field instrument for MMS. *Space Science Reviews*, *199*(1–4), 137–165. https://doi.org/10.1007/s11214-014-0116-9

Lu, S., Wang, R., Lu, Q., Angelopoulos, V., Nakamura, R., Artemyev, A. V., et al. (2020). Onset of magnetotail reconnection by electron kinetics under strong external drive. *Nature Communications*, *11*(1), 1–7. https://doi.org/10.1038/s41467-020-18787-w

Ma, Z. W., & Bhattacharjee, A. (1998). Sudden enhancement and partial disruption of thin current sheets in the magnetotail due to Hall MHD effects. *Geophysical Research Letters*, *25*(17), 3277–3280.

Nakamura, R., Baumjohann, W., Fujimoto, M., Asano, Y., Runov, A., Owen, C. J., et al. (2008). Cluster observations of an ion-scale current sheet in the magnetotail under the presence of a guide field. *Journal of Geophysical Research*, *113*, A07S16. https://doi.org/10.1029/2007JA012760

Nakamura, R., Baumjohann, W., Runov, A., & Asano, Y. (2006). Thin current sheets in the magnetotail observed by cluster. *Space Science Reviews*, *122*(1–4), 29–38.

Norgren, C., Graham, D. B., Khotyaintsev, Y. V., André, M., Vaivads, A., Hesse, M., et al. (2018). Electron reconnection in the magnetopause current layer. *Journal of Geophysical Research: Space Physics*, *123*, 9222–9238. https://doi.org/10.1029/2018JA025676

Paschmann, G., & Schwartz, S. J. (2000). ISSI book on analysis methods for multi-spacecraft data. *ESA Special Publication*, *449*, 99–99.

Petrukovich, A. A., Baumjohann, W., Nakamura, R., & Runov, A. (2008). Formation of current density profile in tilted current sheets. *Annals of Geophysics-Germany*, *26*(12), 3669–3676.

Phan, T. D., Eastwood, J. P., Shay, M. A., Drake, J. F., Sonnerup, B. U. Ö., Fujimoto, M., et al. (2018). Electron magnetic reconnection without ion coupling in Earth's turbulent magnetosheath. *Nature*, *557*(7704), 202–206. https://doi.org/10.1038/s41586-018-0091-5

Pollock, C., Moore, T., Jacques, A., Burch, J., Gliese, U., Saito, Y., et al. (2016). Fast plasma investigation for magnetospheric multiscale. *Space Science Reviews*, *199*(1–4), 331–406. https://doi.org/10.1007/s11214-016-0245-4

Pritchett, P. L., & Lu, S. (2018). Externally driven onset of localized magnetic reconnection and disruption in a magnetotail configuration. *Journal of Geophysical Research: Space Physics*, *123*, 2787–2800. https://doi.org/10.1002/2017JA025094

Pyakurel, P. S., Shay, M. A., Phan, T. D., Matthaeus, W. H., Drake, J. F., TenBarge, J. M., et al. (2019). Transition from ion-coupled to electron-only reconnection: Basic physics and implications for plasma turbulence. *Physics of Plasmas*, *26*(8).

Rager, A. C., Dorelli, J. C., Gershman, D. J., Uritsky, V., Avanov, L. A., Torbert, R. B., et al. (2018). Electron crescent distributions as a manifestation of diamagnetic drift in an electron-scale current sheet: Magnetospheric multiscale observations using new 7.5 ms fast plasma investigation moments. *Geophysical Research Letters*, *45*, 578–584. https://doi.org/10.1002/2017GL076260

Russell, C. T., Anderson, B. J., Baumjohann, W., Bromund, K. R., Dearborn, D., Fischer, D., et al. (2016). The magnetospheric multiscale magnetometers. *Space Science Reviews*, *199*(1–4), 189–256. https://doi.org/10.1007/s11214-014-0057-3

Schwartz, S. J. (1998). *Analysis methods for multi spacecraft data*, *Shock and Discontinuity Normals, Mach Numbers, and Related Parameters* (pp. 249–267). Bern Switzerland: Eur Space Agency.

Sergeev, V. A., Mitchell, D. G., Russell, C. T., & Williams, D. J. (1993). Structure of the tail plasma current sheet at similar-to-11 R(E) and its changes in the course of a substorm. *Journal of Geophysical Research*, *98*(A10), 17,345–17,365.

Shay, M. A., Haggerty, C. C., Phan, T. D., Drake, J. F., Cassak, P. A., Wu, P., et al. (2014). Electron heating during magnetic reconnection: A simulation scaling study. *Physics of Plasmas*, *21*(12).

Shi, Q. Q., Shen, C., Pu, Z. Y., Dunlop, M. W., Zong, Q. G., Zhang, H., et al. (2005). Dimensional analysis of observed structures using multipoint magnetic field measurements: Application to cluster. *Geophysical Research Letters*, *32*, L12105. https://doi.org/10.1029/2005GL022454

Sitnov, M. I., & Schindler, K. (2010). Tearing stability of a multiscale magnetotail current sheet. *Geophysical Research Letters*, *37*, L08102. https://doi.org/10.1029/2010GL042961

Sonnerup, B. U. O. (1979). Magnetic field reconnection. In L. T. Lanzerotti, C. F. Kennel, & E. N. Parker (Eds.), *Solar system plasma physics* (pp. 45–108). New York: North-Holland.

Stawarz, J. E., Eastwood, J. P., Phan, T. D., Gingell, I. L., Shay, M. A., Burch, J. L., et al. (2019). Properties of the turbulence associated with electron-only magnetic reconnection in Earth's magnetosheath. *The Astrophysical Journal Letters*, *877*(2).

Torbert, R. B., Burch, J. L., Phan, T. D., Hesse, M., Argall, M. R., Shuster, J., et al. (2018). Electron-scale dynamics of the diffusion region during symmetric magnetic reconnection in space. *Science*, *362*(6421), 1391–1395. https://doi.org/10.1126/science.aat2998

Vasko, I. Y., Artemyev, A. V., Petrukovich, A. A., Nakamura, R., & Zelenyi, L. M. (2014). The structure of strongly tilted current sheets in the Earth magnetotail. *Annals of Geophysics-Germany*, *32*(2), 133–146.

Vasyliunas, V. M. (1975). Theoretical models of magnetic-field line merging. *Reviews of Geophysics*, *13*(1), 303–336.

Wang, R. S., Lu, Q., Nakamura, R., Baumjohann, W., Huang, C., Russell, C. T., et al. (2018). An electron-scale current sheet without bursty reconnection signatures observed in the near-Earth tail. *Geophysical Research Letters*, *45*, 4542–4549. https://doi.org/10.1002/2017GL076330

Wygant, J. R., Cattell, C. A., Lysak, R., Song, Y., Dombeck, J., McFadden, J., et al. (2005). Cluster observations of an intense normal component of the electric field at a thin reconnecting current sheet in the tail and its role in the shock-like acceleration of the ion fluid into the separatrix region. *Journal of Geophysical Research*, *110*, A09206. https://doi.org/10.1029/2004JA010708

Yamada, M., Kulsrud, R., & Ji, H. T. (2010). Magnetic reconnection. *Reviews of Modern Physics*, *82*(1), 603–664.

Yoo, J., Yamada, M., Ji, H. T., Jara-Almonte, J., & Myers, C. E. (2014). Bulk ion acceleration and particle heating during magnetic reconnection in a laboratory plasma. *Physics of Plasmas*, *21*(5).

Zenitani, S., Hesse, M., Klimas, A., Black, C., & Kuznetsova, M. (2011). The inner structure of collisionless magnetic reconnection: The electron-frame dissipation measure and Hall fields. *Physics of Plasmas*, *18*(12).

Zhou, M., Deng, X. H., Zhong, Z. H., Pang, Y., Tang, R. X., el-Alaoui, M., et al. (2019). Observations of an electron diffusion region in symmetric reconnection with weak guide field. *The Astrophysical Journal*, *870*(1), 34. https://doi.org/10.3847/1538-4357/aaf16f